HHS Public Access

Author manuscript

J Magn Reson Imaging. Author manuscript; available in PMC 2016 November 01.

Published in final edited form as:

J Magn Reson Imaging. 2015 November ; 42(5): 1450–1457. doi:10.1002/jmri.24914.

Assessment of Tumor Response to Oxygen Challenge using Quantitative Diffusion MRI in an animal model

Zhongwei Zhang, MD, PhD[1], **Qing Yuan, PhD**[1], **Heling Zhou, PhD**[1], **Dawen Zhao, MD, PhD**[1], **Li Li, MD**[1], **Jenifer L Gerberich, BS**[1], and **Ralph P Mason, PhD**[1]

[1]Department of Radiology, UT Southwestern Medical Center, Dallas, TX, USA

Abstract

Purpose—To assess tumor response to oxygen challenge using quantitative diffusion MR imaging.

Materials and Methods—A well-characterized Dunning R3327-AT1 rat prostate cancer line was implanted subcutaneously in the right thigh of male Copenhagen rats (N=8). Diffusion-weighted images (DWI) with multiple b values (0, 25, 50, 100, 150, 200, 300, 500, 1000, 1500 s/mm^2) in three orthogonal directions were obtained using a multi-shot FSE-based Stejskal-Tanner DWI sequence (FSE-DWI) at 4.7 T, while rats breathed medical air (21% oxygen) and with 100% oxygen challenge. Stretched-exponential and intravoxel incoherent motion (IVIM) models were used to calculate and compare quantitative diffusion parameters: diffusion heterogeneity index (α), intravoxel distribution of diffusion coefficients (DDC), tissue diffusivity (Dt), pseudo-diffusivity (Dp) and perfusion fraction (f) on a voxel-by-voxel basis.

Results—A significant increase of α (73.9±4.7% in air vs. 78.1±4.5% in oxygen, p = 0.0198) and a significant decrease of f (13.4±3.7% in air vs. 10.4±2.7% in oxygen, p = 0.0201) were observed to accompany oxygen challenge. Correlations between f and α during both air and oxygen breathing were found, the correlation coefficients (r) were −0.90 and −0.96, respectively. Positive correlations between Dt and DDC with oxygen breathing (r = 0.95, p =0.0003), f and DDC with air breathing were also observed (r = 0.95, p =0.0004).

Conclusion—Quantitative diffusion MRI demonstrated changes in tumor perfusion in response to oxygen challenge.

Keywords

Diffusion-weighted imaging; Intravoxel incoherent motion (IVIM); Stretched-exponential model; Perfusion; Tumor Oxygenation; Hyperoxia

Hyperoxia or oxygen gas breathing challenge has been proposed to modify tumor oxygenation for therapy or diagnosis (1). Hyperoxia is consistent with raising the arterial oxygen partial pressure (pO_2) and decreasing deoxy-Hb concentration in blood, thereby enhancing oxygen supply at the capillary and tissue levels (1–3).

Corresponding Author and Reprint Info: Zhongwei Zhang, MD, PhD, Address: 5323 Harry Hines BLVD, Dallas, TX, 75390-9058, USA, Tel: (+1)-214-648-7612, Fax: (+1)-214-648-4538, sljzzw@gmail.com or zhongwei.zhang@utsouthwestern.edu.

Oxygen affects MR signals of blood by two primary physical mechanisms: 1) the paramagnetic property of deoxyhemoglobin (deoxy-Hb) (4), which creates large magnetic susceptibility variations near blood vessels enhancing phase dispersion of water proton signals, thereby accelerating transverse relaxation rate (R_2*), which is often termed a BOLD (blood oxygen level dependent) contrast effect (2). A parabolic relationship between R_2(*) of blood and the fraction of oxygenated hemoglobin relative to the total amount of hemoglobin (Y) is widely reported (5–7); 2) the paramagnetic property of molecular oxygen (8,9). Molecular oxygen increases longitudinal relaxation rate (R_1) due to the dipole-dipole and hyperfine interaction between the proton spins and the unpaired spins of the oxygen molecules (10). A linear relationship between both plasma and whole blood pO_2 changes (i.e., ΔpO_2) and R_1 changes (i.e., ΔR_1) is well-defined (11–13). Although relationships between relaxation rates and blood oxygenation are established, observed MRI signal responses to oxygen inhalation are sometimes confounded in normal tissues and in some tumors (9), (14–16). Responses to oxygen inhalation appear to be tissue-dependent. Interpretation of MRI measurements regarding tumor oxygenation, should optimally consider blood volume and flow since changes in these parameters can counteract the effect of blood oxygenation changes (16,17).

Diffusion weighted MRI (DWI) has provided opportunities to characterize the tumor microenvironment and apparent diffusion coefficient (ADC) has been used for predicting and monitoring tumor response to therapy (18). Intravoxel incoherent motion (IVIM) DWI, as originally described by Le Bihan *et al*. (19), utilizes low b values to sensitize DWI to motions of water within the capillary bed. According to the IVIM DWI model, pure extravascular molecular diffusion and microcirculation of blood within the capillaries (perfusion) can be separated using a biexponential decay function, therefore providing additional parameters for tissue characterization (20,21). IVIM imaging has been validated as a quantitative method to measure perfusion in the human brain under hypercapnia and hyperoxygenation stimuli (22).

Unlike most normal tissues, tumors have a chaotic and poorly regulated blood supply (17). Increased oxygen content of the arterial blood accompanying hyperoxic gas breathing may improve the O_2 diffusion from the microvessel to the cells, but the response to a vasoactive challenge is not always predictable(17,23). We hypothesized that vascular responses caused by hyperoxia might also alter tumor perfusion. Thus, the purpose of this study was to: 1) determine whether a significant response to hyperoxia occurs in tumors using quantitative diffusion MRI; 2) evaluate the possible mechanisms for responses at the microscopic level in a tumor model.

MATERIALS AND METHODS

This study was approved by the Institutional Animal Care and Use Committee. A well-characterized Dunning R3327-AT1 rat prostate cancer line (24,25) was implanted subcutaneously via a small incision in the right thigh of male Copenhagen rats (~270 g, Charles River, Inc., TX), as described in detail previously (26). MRI was performed when tumors reached approximately 1.5~2 cm in diameter. Tumor volume was calculated as: $V = (\pi/6)\times a\times b\times c$, where *a*, *b* and *c* are the three orthogonal diameters measured using a caliper.

MR Imaging

Anesthetized rats were imaged using a horizontal bore 4.7 T MRI scanner (Agilent Technologies Inc., Palo Alto, CA), while breathing air (21% oxygen) followed by 100% oxygen. Anesthesia was induced with isoflurane (5%) and maintained as an isoflurane/gas mixture (1.5% isoflurane at 2 L/min) delivered by a facemask. Anesthetized animals were placed on a plastic bed with a thermal blanket and a warm water flowing system to maintain body temperature. The tumor bearing thighs were placed inside a 35 mm home-built solenoid volume coil. Physiological parameters, including respiratory rate and body temperature, were monitored during MRI using a small animal monitoring and gating system (SA Instruments, Inc., Stony Brook, NY). Physiological parameters for anesthetized rats during MRI acquisition were: respiration rate (25–35 bpm); rectal temperature (36.8±0.4 °C).

Following initial localizer and T_2-weighted anatomical images, Diffusion gradients applied in three orthogonal directions and 10 b values (0, 25, 50, 100, 150, 200, 300, 500, 1000, 1500 s/mm^2) were obtained using a multi-shot FSE-based Stejskal-Tanner DWI sequence (FSE-DWI). Three axial slices of tumor were acquired with thickness = 2 mm, gap = 1 mm, FOV = 40 mm × 40 mm, matrix = 128 × 64, in-plane resolution = 0.31 × 0.63 mm^2, TE/TR = 56/2000 ms, echo train length = 8, Number of average =1 and acquisition time = 6 min 20 seconds. Data were acquired 3 times for each gas, respectively.

Stretched-exponential Model

The stretched-exponential model was developed to describe diffusion-related signal decay as a continuous distribution of sources decaying at different rates without making assumptions about the number of participating sources (27). This model yields a measure of the moments of the intravoxel distribution of diffusion coefficients (DDC) and heterogeneity index (α) in water diffusion (27):

$$\frac{S_b}{S_0} = e^{-(b \cdot DDC)^{\alpha}} \quad [1]$$

where S_b represents the signal intensity for each b value and S_0 is the initial signal intensity at b = 0 s/mm^2. The diffusion-sensitizing factor b depends on the gyromagnetic ratio (γ, 42.58 MHz/T for proton), the duration (δ), strength (G), and interval (Δ) of the magnetic field gradient: $b = \gamma^2 G^2 \delta^2 (\Delta - \delta/3)$. The dimensionless parameter α relating to intravoxel water diffusion heterogeneity (between 0 and 1), characterizes deviation of the signal attenuation from mono-exponential form. α = 1 is equivalent to mono-exponential diffusion-weighted signal decay, hence low intravoxel diffusion heterogeneity, while α close to 0 indicates a higher degree of multi-exponential signal decay. DDC has the properties and units of a standard ADC and can be considered as the composite of individual ADCs weighted by the volume fraction of water in each part of the continuous distribution of ADCs. This model was used to determine whether there was a significant response in diffusion to hyperoxia.

IVIM Model

The IVIM model accounts for both diffusion and perfusion effects on the signal decay (19),

$$\frac{S_b}{S_0}=(1-f)\cdot e^{-b\cdot Dt}+f\cdot e^{-b\cdot Dp} \quad [2]$$

where f is the perfusion fraction, Dt is the diffusion coefficient and Dp is the pseudodiffusion coefficient. The parameters in the model were estimated using a segmented IVIM analysis to ensure a more robust analysis compared to an unconstrained fit (28,29). Briefly, in the first step, the curve was fitted for Dt using those b values greater than approximately 1/Dp (b> 250 s/mm^2 used in this study) (30). The assumption for this step was that Dp is significantly greater than Dt, so that the influence of Dp on signal decay can be neglected for b factors greater than 1/Dp. In the second step, the curve was fitted for f and Dp for all the b values, while keeping the Dt calculated in first step constant. This model was used to measure possible perfusion responses to hyperoxia at the microscopic level.

Data Processing

Image analysis was performed off-line using Matlab (Mathworks, Natick, MA) procedures developed in house.

Quantitative diffusion parameters, including α, DDC, Dt, Dp, and f were calculated on a voxel-by-voxel basis. For each tumor, a region of interest (ROI) was drawn on the first DWI image (S_b=0), and then copied to all diffusion parametric maps. The mean values of measured diffusion parameters for each tumor are reported. The pair-wise comparisons were made between air and oxygen breathing using two-tailed Student's t tests.

Correlations between parameters (α, DDC) derived from stretched-exponential model and parameters (Dt, Dp, and f) derived from IVIM model were investigated. A p <0.05 was considered statistically significant.

Histology

Approximately one hour after MRI, the rats were re-anesthetized and injected IV with the perfusion marker Hoechst 33342 (Life Technologies, Carlsbad, CA) at a dose of 10 mg/kg. Approximately one minute after injection, blood flow to the tumor was cut off with a zip tie situated proximal to the tumor on the leg. The tumor was then excised and bisected along the MR imaging plane. Animals were euthanized following this procedure. Tumor was placed in Tissue-Tek O.C.T. compound, frozen in liquid nitrogen and stored at −80 °C. Histological examinations were performed on sections corresponding to the slice acquired by MRI. Hoechst 33342 fluorescent microscopic images were processed using Zen software (Blue Edition 2012, Jena, Germany). All Histological examinations were evaluated by an experienced observer (L.L. who had 15 years' experience) who was blinded to any MRI data.

RESULTS

Representative parametric maps derived from stretched-exponential model (i.e., α and DDC) and IVIM model (i.e., f, Dp and Dt) with both air and oxygen breathing were shown in Figure 1.

For the group of 8 tumors, there was a significant increase in α (73.9±4.7 with air to 78.1±4.5 with O_2, $p < 0.05$) and a significant decrease of perfusion fraction f (13.4±3.7 to 10.4±2.7, $p < 0.05$) (Table 1 and Fig.2). However, no significant response was found in other parameters to oxygen breathing.

Correlations between parameters derived from stretched-exponential model (α, DDC) and parameters derived from IVIM model (Dt, Dp, and f) are listed in Table 2. Significant negative correlations were found between f and α during both air and oxygen breathing with Pearson correlation coefficients $r = -0.90$ ($p = 0.002$ for baseline air) and $r = -0.96$ ($p < 0.001$ with O_2), respectively (Fig.3). Significant positive correlations were also found between DDC and Dt ($r = 0.95$, $p < 0.001$) with oxygen breathing, DDC and f ($r = 0.95$, $p < 0.001$) with air breathing.

Heterogeneity of perfusion fraction assessed by MRI coincided with the distribution of Hoechst 33342 observed in the excised tumors. Hoechst staining and perfusion fraction obtained by MRI are shown for representative tumor (#4) (Fig.4). Two regions with distinct Hoechst 33342 uptake were shown with high magnification (Fig. 4D and E). Hoechst 33342 uptake was visibly higher for region in Fig. 4D, represented an increase in uptake two times than region in Fig. 4E.

DISCUSSION

MRI allows noninvasive monitoring and quantification of tumor diffusion. Quantitative diffusion parameters were successfully calculated in this study using the stretched-exponential and IVIM models during air and oxygen breathing. Inhalation of oxygen caused significant increase of intra-voxel water diffusion heterogeneity and a small, but statistically significant decrease of perfusion fraction in the AT1 tumor. However, no significant changes in overall tumor perfusion-free diffusion (Dt) were observed.

Inhalation of 100% oxygen elevates arterial plasma pO_2 at the level of the proximal arterioles, but the physiological changes due to hyperoxia are organ-specific and have a complex relationship to perfusion and metabolic demand (9). The current findings demonstrate that a significant physiological response to hyperoxia exists at the microscopic level, consistent with previous work on vascular function and maturation study (31).

In this study, a significant increase in intra-voxel water diffusion heterogeneity α with oxygen breathing suggests that multiple sources decaying at different rates at the intra-voxel level can be detected and this differential should represent tissue water diffusion changes, either perfusion-induced or diffusion-induced, based on the stretched-exponential model. The significant negative correlations found between f and α during both air and oxygen breathing, suggest that the intravoxel heterogeneity of signal decay was strongly influenced

by the perfusion effect. This is consistent with intravoxel heterogeneity in vascular structures leading to the existence of a high number of sources decaying at different rates (i.e. lower α values). An increased perfusion fraction will result in an increase of intravoxel heterogeneity.

The tissue microvasculature can be divided into flow controlling vessels and distribution vessels controlled by autoregulation, as well as humoral and neural factors (32). For normal tissues, oxygen has been reported to cause arteriolar vasoconstriction and tissue perfusion changes (33). However, tumors develop in complex tissue environments and tumor blood vessels have been described as chaotic, larger in diameter than normal vessels, longer in length with increased tortuosity and permeability (34). Although tumors have immature and leaky blood vessels, a significant decrease of perfusion fraction while breathing oxygen was observed suggesting that a tumor vascular response to oxygen occurs. The perfusion changes mediated by oxygen-induced vasoconstriction may lessen the ratio of blood to tissue within a given voxel. This study suggests that quantitative diffusion MRI might act as a sensitive method for assessment of tumor responses to oxygen challenge. Note that an increased perfusion fraction was observed in one tumor(#8), it maybe result from more opening of previously closed capillaries to increase the organ's total capillary surface area by capillary recruitment mechanism during oxygen inhalation (35).

A previous study reported a positive correlation between ADC and tissue pO_2 in a RIF-1 tumor model (36), but another study (37) found no such correlation between ADC and pO_2 in the same tumor model. However, both studies were lack of perfusion measurement. We found no significant changes of Dt, supporting the independence of the tissue diffusion coefficient in the non-perfused compartment while breathing oxygen. Significant positive correlations between DDC and Dt with oxygen breathing, DDC and f with air breathing, were found and these findings suggest that DDC is a weighted sum over a distribution of ADCs that comprise the multi-exponential decay properties (i.e. extravascular diffusion and perfusion components in IVIM model). A significant decrease of perfusion without notable changes of diffusion component will alter the relative contributions to DDC from the two components in IVIM model. Therefore, in order to relate changes in ADC values with changes in tumor oxygenation, the perfusion contribution should be taken into consideration.

Although this study aimed to assess tumor physiological responses to oxygen challenge using quantitative diffusion MR imaging, there are a few limitations. First, quantitative diffusion-derived parameters were only measured in three slices for each tumor with 2D acquisition due to time constraints. To further analyze the whole tumor responses, fast 3D high resolution acquisition would be needed to extend volume coverage. Second, the sample size is small and limited to a single tumor type in the current study. Third, perfusion fraction has so far only been validated using the perfusion marker Hoechst 33342 with no attempt to differentiate air and oxygen breathing. In-vivo validation methods such as intravital microscopy and near-infrared spectroscopy should be performed in future studies (31,38).

In conclusion, quantitative diffusion MRI suggests that there are tumor-dependent physiological responses to hyperoxia. The current study demonstrated quantitative diffusion

MRI as a noninvasive and sensitive method for assessment of tumor perfusion responses to oxygen challenge.

ACKNOWLEDGEMENTS

The authors are grateful to Dr. Peter Peschke (DKFZ) for providing tumor cells and Rebecca Denney for assistance in physiological monitoring.

Grant Information: This work was supported in part by NIH R01 CA139043, P41 EB015908 & P30 CA142543.

REFERENCES

1. Tatum JL, Kelloff GJ, Gillies RJ, et al. Hypoxia: Importance in tumor biology, noninvasive measurement by imaging, and value of its measurement in the management of cancer therapy. Int J Radiat Biol. 2006; 82:699–757. [PubMed: 17118889]
2. Overgaard J. Clinical-Evaluation of Nitroimidazoles as Modifiers of Hypoxia in Solid Tumors. Oncol Res. 1994; 6:509–518. [PubMed: 7620219]
3. Robinson SP, Collingridge DR, Howe FA, Rodrigues LM, Chaplin DJ, Griffiths JR. Tumour response to hypercapnia and hyperoxia monitored by FLOOD magnetic resonance imaging. NMR Biomed. 1999; 12:98–106. [PubMed: 10392806]
4. Ogawa S, Lee TM, Kay AR, Tank DW. Brain magnetic resonance imaging with contrast dependent on blood oxygenation. Proc Natl Acad Sci USA. 1990; 87:9868–9872. [PubMed: 2124706]
5. Wright GA, Hu BS, Macovski A. Estimating oxygen saturation of blood in vivo with MR imaging at 1.5 T. J Mag Reson Imaging. 1991; 1:275–283.
6. Silvennoinen MJ, Clingman CS, Golay X, Kauppinen RA, van Zijl PC. Comparison of the dependence of blood R2 and R2* on oxygen saturation at 1.5 and 4.7 Tesla. Magn Reson Med. 2003; 49:47–60. [PubMed: 12509819]
7. Zhao JM, Clingman CS, Narvainen MJ, Kauppinen RA, van Zijl PC. Oxygenation and hematocrit dependence of transverse relaxation rates of blood at 3T. Magn Reson Med. 2007; 58:592–597. [PubMed: 17763354]
8. Edelman RR, Hatabu H, Tadamura E, Li W, Prasad PV. Noninvasive assessment of regional ventilation in the human lung using oxygen-enhanced magnetic resonance imaging. Nature Med. 1996; 2:1236–1239. [PubMed: 8898751]
9. O'Connor JP, Jackson A, Buonaccorsi GA, et al. Organ-specific effects of oxygen and carbogen gas inhalation on tissue longitudinal relaxation times. Magn Reson Med. 2007; 58:490–496. [PubMed: 17763345]
10. Mirhej ME. Proton Spin Relaxation by Paramagnetic Molecular Oxygen. Can J Chem. 1965; 43:1130–1138.
11. d'Othee JB, Rachmuth G, Munasinghe J, Lang EV. The effect of hyperoxygenation on T1 relaxation time in vitro. Acad Radiol. 2003; 10:854–860. [PubMed: 12945919]
12. Zaharchuk G, Busse RF, Rosenthal G, Manley GT, Glenn OA, Dillon WP. Noninvasive oxygen partial pressure measurement of human body fluids in vivo using magnetic resonance imaging. Acad Radiol. 2006; 13:1016–1024. [PubMed: 16843855]
13. Kershaw LE, Naish JH, McGrath DM, Waterton JC, Parker GJM. Measurement of Arterial Plasma Oxygenation in Dynamic Oxygen-Enhanced MRI. Magn Reson Med. 2010; 64:1838–1842. [PubMed: 20677232]
14. Tadamura E, Hatabu H, Li W, Prasad PV, Edelman RR. Effect of oxygen inhalation on relaxation times in various tissues. J Magn Reson Imaging. 1997; 7:220–225. [PubMed: 9039619]
15. Cheng HL. Effect of hyperoxia and hypercapnia on tissue oxygen and perfusion response in the normal liver and kidney. PloS One. 2012; 7:e40485. [PubMed: 22792349]
16. Christen T, Lemasson B, Pannetier N, et al. Is T2* enough to assess oxygenation? Quantitative blood oxygen level-dependent analysis in brain tumor. Radiology. 2012; 262:495–502. [PubMed: 22156990]

17. Howe FA, Robinson SP, McIntyre DJO, Stubbs M, Griffiths JR. Issues in flow and oxygenation dependent contrast (FLOOD) imaging of tumours. NMR Biomed. 2001; 14:497–506. [PubMed: 11746943]
18. Li SP, Padhani AR. Tumor response assessments with diffusion and perfusion MRI. J Magn Reson Imaging. 2012; 35:745–763. [PubMed: 22434697]
19. Le Bihan D, Breton E, Lallemand D, Aubin ML, Vignaud J, Laval-Jeantet M. Separation of diffusion and perfusion in intravoxel incoherent motion MR imaging. Radiology. 1988; 168:497–505. [PubMed: 3393671]
20. Koh DM, Collins DJ, Orton MR. Intravoxel incoherent motion in body diffusion-weighted MRI: reality and challenges. AJR. 2011; 196:1351–1361. [PubMed: 21606299]
21. Shinmoto H, Tamura C, Soga S, et al. An intravoxel incoherent motion diffusion-weighted imaging study of prostate cancer. AJR. 2012; 199:496–500.
22. Federau C, Maeder P, O'Brien K, Browaeys P, Meuli R, Hagmann P. Quantitative measurement of brain perfusion with intravoxel incoherent motion MR imaging. Radiology. 2012; 265:874–881. [PubMed: 23074258]
23. Jordan BF, Crokart N, Baudelet C, Cron GO, Ansiaux R, Gallez B. Complex relationship between changes in oxygenation status and changes in R2(*): The case of insulin and NS-398, two inhibitors of oxygen consumption. Magn Reson Med. 2006; 56:637–643. [PubMed: 16897769]
24. Isaacs JT, Isaacs WB, Feitz WFJ, Scheres J. Establishment and Characterization of 7 Dunning Rat Prostatic-Cancer Cell-Lines and Their Use in Developing Methods for Predicting Metastatic Abilities of Prostatic Cancers. Prostate. 1986; 9:261–281. [PubMed: 3774632]
25. Peschke P, Lohr F, Hahn EW, et al. Response of the rat Dunning R3327-AT1 prostate tumor to treatment with fractionated fast neutrons. Radiat Res. 1992; 129:112–114. [PubMed: 1728053]
26. Hahn EW, Peschke P, Mason RP, Babcock EE, Antich PP. Isolated Tumor-Growth in a Surgically Formed Skin Pedicle in the Rat - a New Tumor-Model for Nmr-Studies. Magn Reson Imaging. 1993; 11:1007–1017. [PubMed: 8231664]
27. Bennett KM, Schmainda KM, Bennett RT, Rowe DB, Lu H, Hyde JS. Characterization of continuously distributed cortical water diffusion rates with a stretched-exponential model. Magn Reson Med. 2003; 50:727–734. [PubMed: 14523958]
28. Chandarana H, Lee VS, Hecht E, Taouli B, Sigmund EE. Comparison of biexponential and monoexponential model of diffusion weighted imaging in evaluation of renal lesions: preliminary experience. Invest Radiol. 2011; 46:285–291. [PubMed: 21102345]
29. Notohamiprodjo M, Chandarana H, Mikheev A, et al. Combined intravoxel incoherent motion and diffusion tensor imaging of renal diffusion and flow anisotropy. Magn Reson Med. 2014
30. Sigmund EE, Vivier PH, Sui D, et al. Intravoxel Incoherent Motion and Diffusion-Tensor Imaging in Renal Tissue under Hydration and Furosemide Flow Challenges. Radiology. 2012; 263(3):758–769. [PubMed: 22523327]
31. Neeman M, Dafni H, Bukhari O, Braun RD, Dewhirst MW. In vivo BOLD contrast MRI mapping of subcutaneous vascular function and maturation: Validation by intravital microscopy. Magn Reson Med. 2001; 45:887–898. [PubMed: 11323816]
32. Nathan AT, Singer M. The oxygen trail: tissue oxygenation. Brit Med Bull. 1999; 55:96–108. [PubMed: 10695081]
33. Messina EJ, Sun D, Koller A, Wolin MS, Kaley G. Increases in Oxygen-Tension Evoke Arteriolar Constriction by Inhibiting Endothelial Prostaglandin Synthesis. Microvasc Res. 1994; 48:151–160. [PubMed: 7854203]
34. Gillies RJ, Raghunand N, Karczmar GS, Bhujwalla ZM. MRI of the tumor microenvironment. J Magn Reson Imaging. 2002; 16:430–450. [PubMed: 12353258]
35. Jespersen SN, Ostergaard L. The roles of cerebral blood flow, capillary transit time heterogeneity, and oxygen tension in brain oxygenation and metabolism. J Cereb Blood Flow Metab. 2012; 32(2):264–277. [PubMed: 22044867]
36. Dunn JF, Ding S, O'Hara JA, et al. The apparent diffusion constant measured by MRI correlates with pO2 in a RIF-1 tumor. Magn Reson Med. 1995; 34:515–519. [PubMed: 8524017]
37. Helmer KG, Han S, Sotak CH. On the correlation between the water diffusion coefficient and oxygen tension in RIF-1 tumors. NMR Biomed. 1998; 11(3):120–130. [PubMed: 9699495]

38. Liu HL, Song YL, Worden KL, Jiang X, Constantinescu A, Mason RP. Noninvasive investigation of blood oxygenation dynamics of tumors by near-infrared spectroscopy. Appl Optics. 2000; 39:5231–5243.

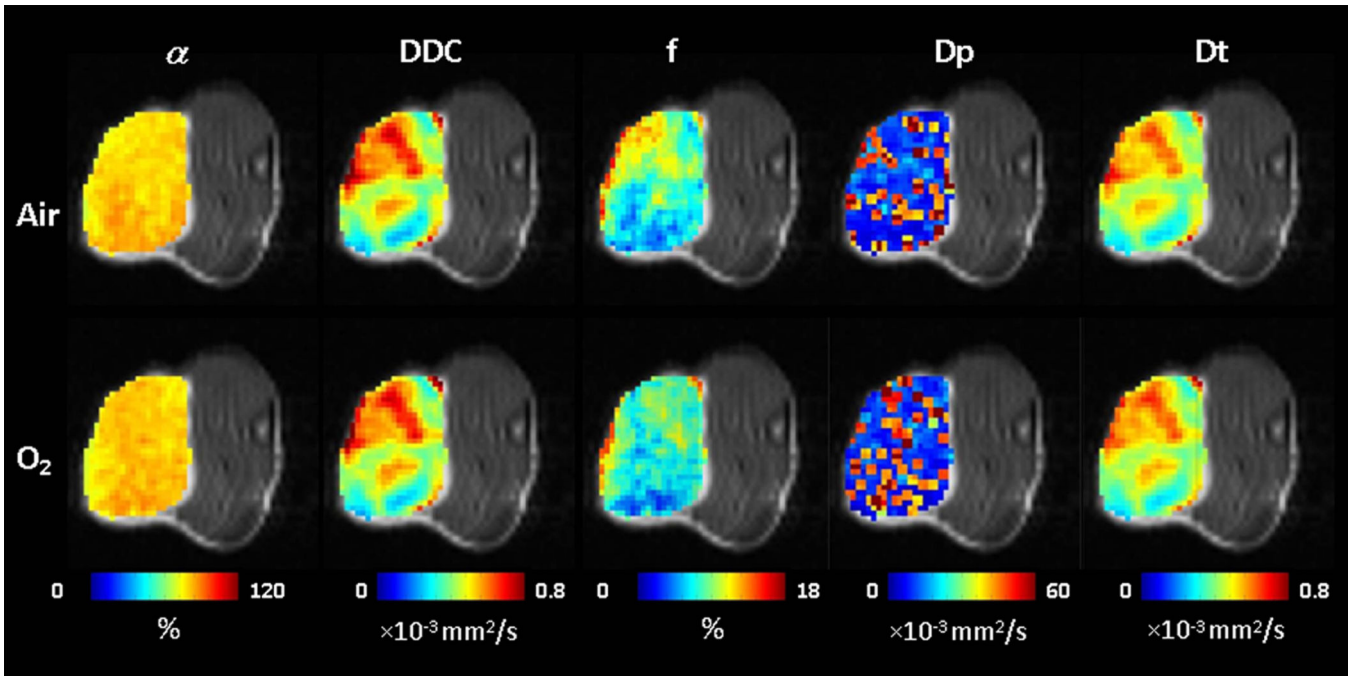

Fig.1.

Quantitative diffusion parametric maps overlaid on DWI (S_b = 0) images of Dunning prostate R3327-AT1 tumor growing subcutaneously in rat thigh (tumor#4). Extensive intra-tumor heterogeneity is seen in each parameter map both for baseline and with oxygen breathing challenge. (α: Heterogeneity index; DDC: Distribution of Diffusion Coefficient; f: Perfusion fraction; Dp: pseudo-diffusion coefficient; Dt: tissue diffusion coefficient)

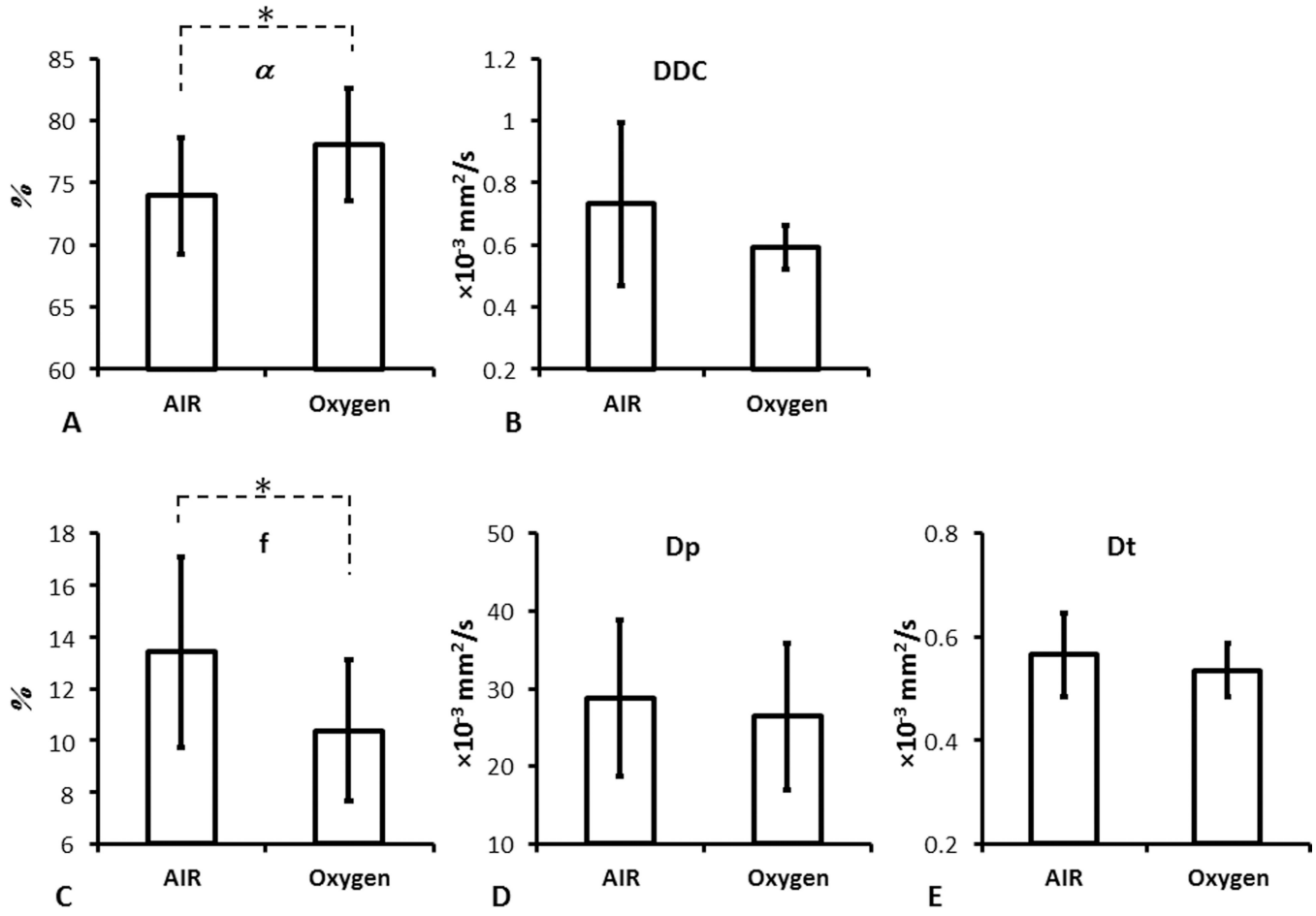

Fig.2.

The measured diffusion parameters for the entire tumor during air and oxygen inhalation. A) α; B) DDC; C) f; D) Dp; E) Dt. A significant increase of α and decrease of f was observed accompanying oxygen challenge. Mean ± standard deviation is shown (N = 8 tumors; * $p < 0.05$)

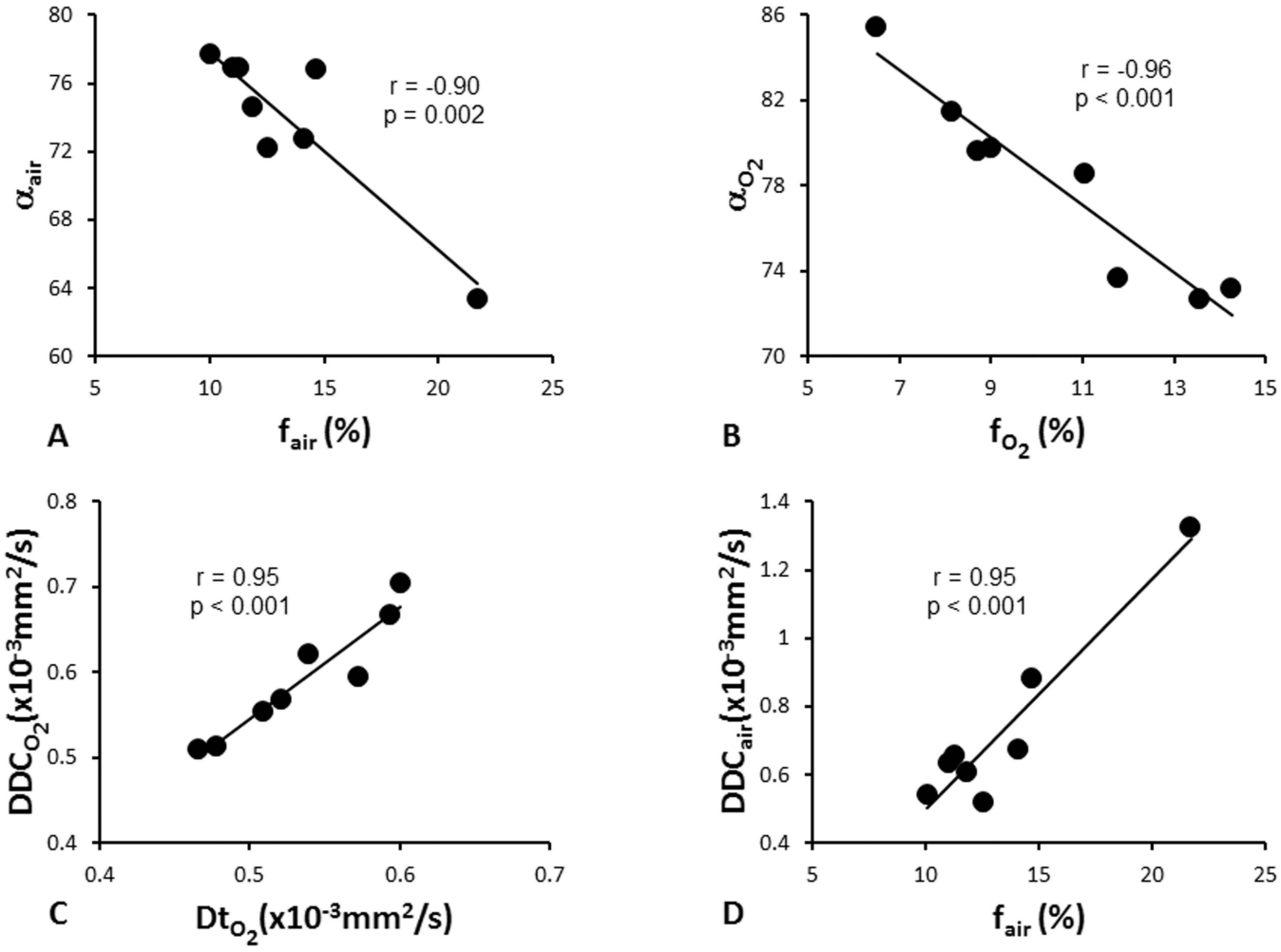

Fig.3.

Correlations among diffusion parameters derived from stretched-exponential and IVIM models. A) f vs. α with air breathing; B) f vs. α with oxygen breathing; C) Dt vs. DDC with oxygen breathing; D) f vs. DDC with air breathing.

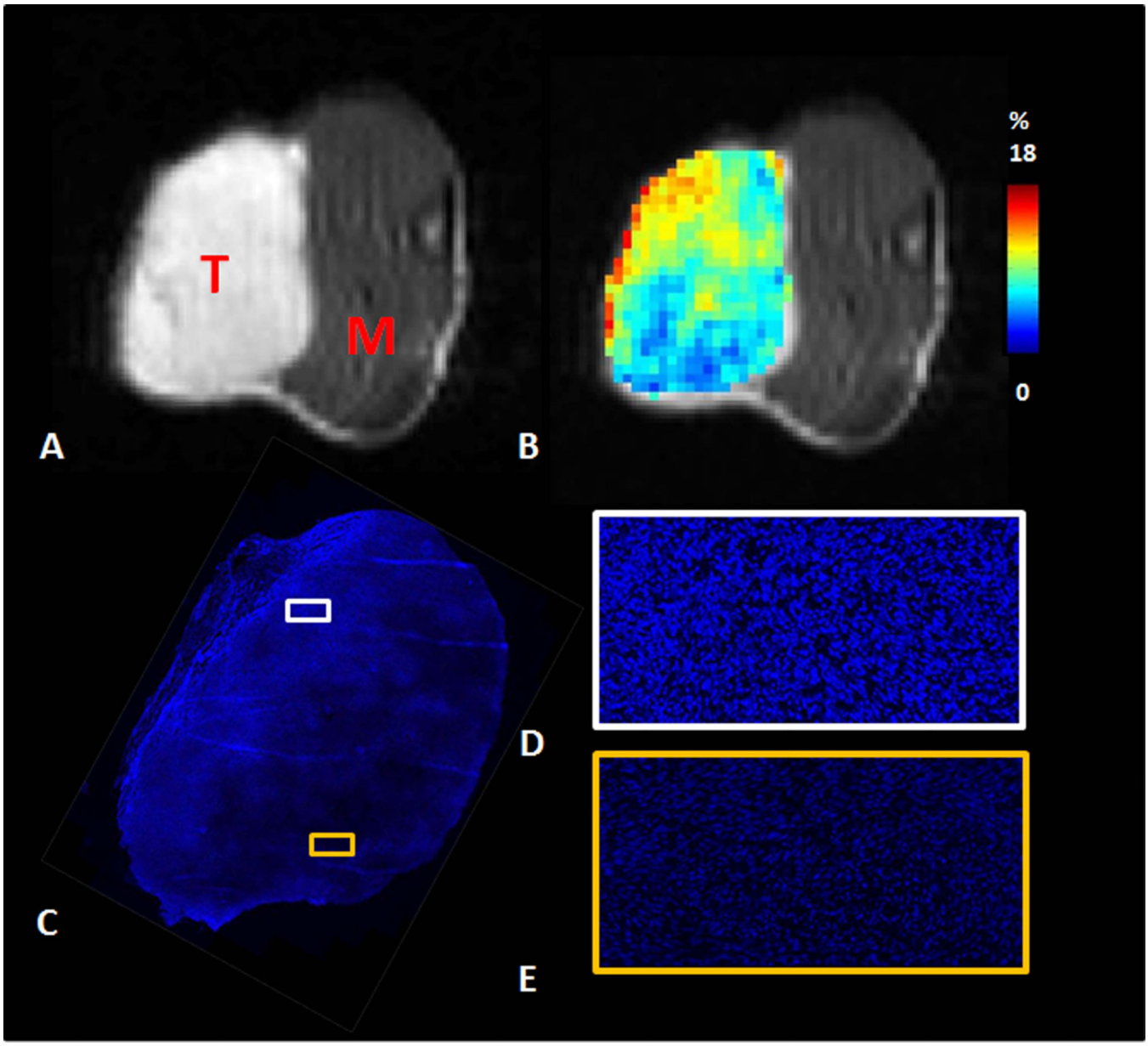

Fig.4.

Perfusion fraction assessed by IVIM coincided with distribution of Hoechst 33342. A) FSE-DWI b_0 image (T: tumor; M: muscle); B) perfusion fraction map derived from IVIM model; C) Hoechst 33342 staining, with representative higher resolution insets showing regions of high perfusion (D) and low perfusion (E), respectively.

Table 1

The measured diffusion parameters in the ROI of the entire tumor presented for each tumor during air and oxygen breathing.

Rat Number	Tumor size(cm^3)	Gas	α (%)	DDC ($\times10^{-3}$ mm^2/s)	Dt ($\times10^{-3}$ mm^2/s)	Dp ($\times10^{-3}$ mm^2/s)	f (%)
1	1.9	Air	76.8±9.6	0.88±0.05	0.74±0.09	41.1±29.9	14.7±4.8
		O_2	79.6±9.6*	0.51±0.04*	0.48±0.03*	12.3±11.1*	8.7±4.5*
2	1.3	Air	76.9±6.5	0.66±0.08	0.59±0.07	39.4±22.7	11.3±2.7
		O_2	79.8±10.7*	0.55±0.06*	0.51±0.05*	17.1±18.5*	9.0±4.7*
3	1.2	Air	72.8±5.9	0.67±0.06	0.57±0.07	29.1±13.8	14.1±2.8
		O_2	73.6±2.7*	0.51±0.05*	0.47±0.05	22.0±20.3*	11.8±1.8
4	1.9	Air	72.2±2.8	0.52±0.08	0.47±0.05	38.2±31.0	12.5±2.2
		O_2	78.6±2.5	0.67±0.04	0.59±0.04*	30.37±11.5	11.1±1.7*
5	1.6	Air	76.9±6.2	0.64±0.04	0.57±0.05	26.6±25.2	11.0±3.0
		O_2	85.4±1.8*	0.59±0.06*	0.57±0.05*	35.7±12.4	6.5±0.9*
6	2.7	Air	77.7±3.2	0.54±0.06	0.50±0.05	21.8±22.0	10.1±1.0
		O_2	81.4±4.3*	0.57±0.08*	0.52±0.01*	36.8±20.8*	8.2±1.9*
7	1.9	Air	63.4±5.2	1.33±0.44	0.54±0.12	13.2±9.1	21.8±3.4
		O_2	73.2±3.1*	0.70±0.06*	0.60±0.05*	21.3±12.1	14.3±2.0*
8	2.5	Air	74.6±4.7	0.61±0.09	0.55±0.06	20.4±14.1	11.9±3.1
		O_2	72.7±4.2*	0.62±0.08*	0.54±0.05*	35.4±24.1	13.6±2.9*
Mean±SD		Air	73.9±4.7	0.73±0.26	0.56±0.08	28.7±10.1	13.4±3.7
		O_2	78.1±4.5	0.59±0.07	0.54±0.05	26.4±9.4	10.4±2.7
p value			0.0198*	0.1569	0.5107	0.7037	0.0201*

Note:

Data are means ± standard deviation, obtained by averaging the values obtained on a voxel-by-voxel basis over three image slices of the entire tumor; Paired t-tests were performed on inter-tumor and intra-tumor levels.

* $p < 0.05$

J Magn Reson Imaging. Author manuscript; available in PMC 2016 November 01.

Table 2

Correlations between parameters (α, DDC) derived from stretched-exponential model and parameters (Dt, Dp, and f) derived from IVIM model.

Measurement	α		DDC	
	Coefficient (r)	**P value**	**Coefficient (r)**	**P value**
Dt	Air: 0.29 O_2 0.03	Air: 0.49 O_2 0.94	Air: 0.29 O_2 0.95	Air: 0.49 O_2 0.0003*
Dp	Air: 0.53 O_2 0.21	Air: 0.18 O_2 0.61	Air: −0.41 O_2 0.36	Air: 0.31 O_2 0.38
f	Air: −0.90 O_2 −0.96	Air: 0.002* O_2 0.0002*	Air: 0.95 O_2 0.52	Air: 0.0004* O_2 0.18

* $p < 0.05$